Int J Adv Manuf Technol (2017) 91:3315–3326
DOI 10.1007/s00170-017-0037-3

ORIGINAL ARTICLE

A novel approach of high-performance grinding using developed diamond wheels

Zhenyu Zhang [1,2] · Siling Huang [1] · Shaochen Wang [1] · Bo Wang [1] · Qian Bai [1] · Bi Zhang [1,3] · Renke Kang [1] · Dongming Guo [1]

Received: 14 November 2016 / Accepted: 9 January 2017 / Published online: 22 January 2017
© Springer-Verlag London 2017

Abstract A novel approach of high-performance grinding is proposed using developed diamond wheels, to obtain minimally damaged surface layer in silicon wafers. For this reason, resin bond diamond wheels are specifically developed with lanthanum oxide (La_2O_3), magnesium oxide (MgO), and ceria (CeO_2) as additives, respectively. The wheels contain grains with a mesh number of 20,000 and a volume fraction of diamond grains of 37.5%. The diamond wheel with ceria additives demonstrates the best grinding performance in terms of surface integrity and roughness. It allows to generate an amorphous surface layer of 43 nm in thickness, without grinding damage beneath in a silicon wafer. This is different from previous reports, in which an amorphous layer is at the top, followed by a damaged crystalline layer underneath induced by a diamond wheel. Below the amorphous layer is the pristine crystalline lattice, which is confirmed using the high-resolution transmission electron microscopy (HRTEM). The ceria wheel results in a surface roughness R_a of 0.88 nm and a peak-to-valley (PV) value of 8.3 nm over an area of 70 × 50 μm^2 on a Si wafer at a feed rate of 15 μm/min.

Keywords Si wafer · Diamond wheel · CeO_2 · Amorphous layer · Transmission electron microscopy

✉ Zhenyu Zhang
zzy@dlut.edu.cn

[1] Key Laboratory for Precision and Non-Traditional Machining Technology of Ministry of Education, Dalian University of Technology, Dalian 116024, China

[2] Changzhou Institute of Dalian University of Technology, Changzhou 213164, China

[3] Department of Mechanical Engineering, University of Connecticut, Storrs, CT 06269, USA

1 Introduction

Silicon (Si) wafers are employed to manufacture more than 90% of the semiconductor devices and have become the foundation of the electronics industry, which is the largest industry in the world [1, 2]. Because of its intrinsic properties and abundance, Si has dominated the semiconductor industry [3]. Nonetheless, Si has hard and brittle nature, compared to those materials with soft and brittle characteristics [4, 5], making it become a hard-to-machine material. Grinding is widely used in the ultraprecision machining of Si wafers due to its advantages in efficiency and form accuracies [6–10]. A stringent requirement is to reduce the manufacturing cost of the Si wafers in a yearly basis. Meanwhile, there is also a machining requirement for a damage-free surface layer with surface roughness of 1-nm level or better. This is a challenge for ultraprecision grinding of Si wafers.

To develop a novel approach of high-performance grinding with minimally damaged surface layer, researchers worldwide have investigated the fundamental material removal mechanisms in precision and ultraprecision grinding of Si wafers using a diamond tip [11–15]. For instance, indentation with a diamond tip is often used to simulate the grinding process in which surface layer damage is unavoidable, although it is merely a quasi-static process. Scratching with a single-point diamond is also used to simulate the grinding process, which is much better than indentation in terms of its dynamic loading. In the nanoscratching process, scratching speed is at the level of micrometer per second. The scratched surface layer is formed with an amorphous layer at the top, followed by a crystalline damaged layer beneath, which is identified in nanoindentation [11, 12], nanoscratch [13–15], and ultraprecision grinding [6, 16, 17]. In addition, high-pressure phases of Si-III (a BC8 phase with the body-centered cubic lattice structure) and Si-XII (an R8 phase with the rhombohedral

lattice structure) [14, 15] are reported in nanoindentation [11, 12] and nanoscratch [14, 15]. Therefore, it is intriguing to obtain solely amorphous layer in Si wafers without damaged crystalline layer for the perfect grinding performance, which is not reported by a diamond wheel.

Grinding is used as a machining tool to obtain minimally damaged surface layer in Si wafers, which is significant to save the cost for the subsequent chemical mechanical polishing, as well as for the semiconductor and microelectronics industries. In this study, a novel approach of high-performance grinding is proposed for acquiring such a surface using ultraprecision grinding. This refers to the high-performance grinding, compared to grinding with conventional diamond wheels. The study also investigates grinding mechanisms and characterizes the ground Si wafers using the high-resolution transmission electron microscopy (HRTEM).

2 Experimental details

The Si wafers used in this study were commercial products (GRINM Advanced Materials Co., Ltd.) of the (100) crystalline plane. The wafers were subjected to chemical mechanical polishing with surface roughness R_a and peak-to-valley (PV) values of 0.37 ± 0.04 nm and 3.6 ± 0.3 nm, respectively, over a measurement area of 70 × 50 μm^2. Three kinds of diamond wheels were developed using additives of lanthanum oxide (La_2O_3), magnesium oxide (MgO), and ceria (CeO_2), which are designated as samples L1, M2, and C3, respectively, as listed in Table 1. The volume percentage of the additives varied from 12.5 to 13.5%. The mesh size of all the three diamond wheels was 20,000, equivalent to an equivalent grain diameter of 760 nm. The grain diameter was consistent with the radius of the single-point diamond tips varying from 744 to 786 nm in the high-speed scratching [7, 8], in which a solely amorphous layer was reported. The concentration of diamond grains in each wheel was 150, equivalent to a volume fraction of 37.5%. Phenolic resin was used as the bond material. Firstly, diamond grains, phenolic resin, and additives were mixed uniformly and then pressed at the room temperature in dies into blocks with dimensions of 18 × 3 × 8 mm^3. The blocks were sintered at a temperature ranging from 200 to 240 °C. A diamond wheel was composed of 48 blocks, distributing uniformly in the groove of an aluminum alloy wheel with a diameter of 350 mm, as shown in Fig. 1. The blocks were glued in the groove with a depth of 3 mm and a width of 3.5 mm, resulting in a height of 5 mm exposed outside. Hence, a diamond wheel was fabricated and fixed on the air spindle of an ultraprecision grinder (Okamoto, VG401 MKII, Japan) with a face runout of 50 nm, as illustrated in Fig. 1b. Prior to grinding, truing was employed to flatten the diamond wheel and make it perpendicular to the axis of the air spindle. Silicon carbide (SiC) powders with mesh size of 400 were used for truing, equivalent to an average grain diameter of 38 μm (Fig. 2a). The SiC powders were characterized using the field emission environmental scanning electron microscopy (SEM, FEI, Quanta 200 FEG, Netherlands), equipped with energy-dispersive spectroscopy (EDS). Deionized water was used to prepare the SiC paste for truing the diamond wheel, as illustrated in Fig. 2b. After truing, a Si wafer was fixed on the vacuum chuck, as displayed in Fig. 1b. During grinding, the diamond wheel and table speeds were set at 43.94 m/s and 120 rpm, respectively. The coolant was deionized water to decrease the grinding temperature for both the diamond wheels and Si wafers. Additionally, the air spindle fed only vertically, guaranteeing the grinding accuracy. After grinding, the surface roughness R_a and PV of Si wafers were measured using the precision noncontact surface profilometry (Zygo, NewView 5022, USA). Cross sections of the Si wafers were characterized using the high-resolution transmission electron microscopy (TEM, FEI, Tecnai F20, Netherlands) and ultrahigh resolution TEM (JEOL, JEM-ARM200F, Japan). The TEM samples were prepared using the focused ion beam technique (FEI, Helios 600i, Netherlands) and then thinned by a Gatan Model 691 precision ion polishing system. The elastic modulus and hardness of sample C3 were measured using a nanomechanical test instrument (TI 950, TriboIndenter®, Hysitron, Minneapolis), at a peak load of 4 N by a developed Berkovich indenter with a tip radius of 398 nm [7, 8]. During indentation, loading, dwelling, and unloading time were 5, 2, and 5 s, respectively.

Table 1 Details of developed diamond wheels and their feed rates

Sample	Additive (wt%)	Additive (vol%)	Resin bond (vol%)	Feed rate (μm/min)
L1	La_2O_3 25.1	La_2O_3 13.5	49	3, 5, 8, 10
M2	MgO 13	MgO 12.5	50	3, 5, 8, 10, 15, 20
C3	CeO_2 25.5	CeO_2 12.5	50	3, 5, 8, 10, 15, 20

3 Results

Figure 3 shows the optical and SEM images of sample L1; its EDS spectrum; optical and SEM images on a ground Si wafer; and surface roughness, arithmetic

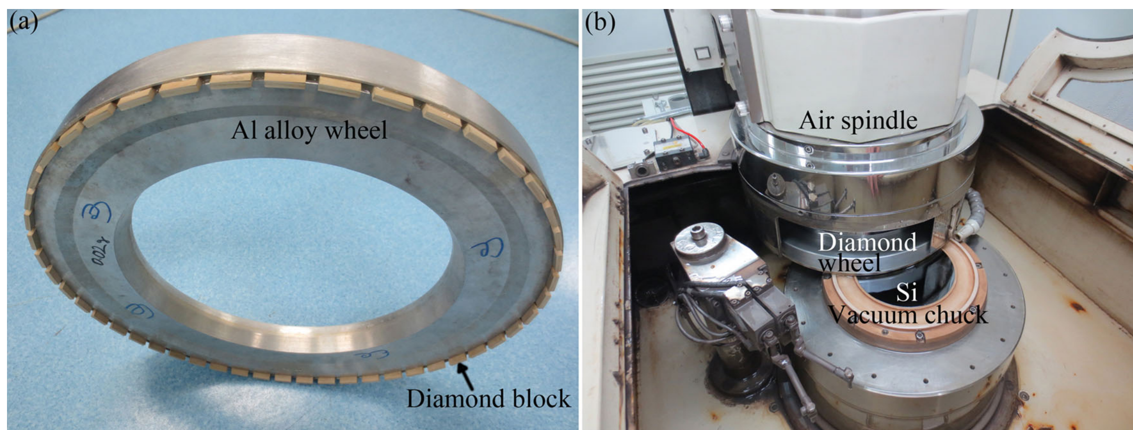

Fig. 1 Optical images of **a** sample C3 fixed on **b** an ultraprecision grinder

average value (R_a), and PV as a function of feed rate on the Si wafers ground by sample L1. The weight percentage of lanthanum oxide (La_2O_3) in sample L1 is 25.1% (Table 1), which is confirmed in Fig. 3c. Consequently, La_2O_3 is observed in Fig. 3b marked by black arrows. The La_2O_3 powders agglomerated, indicating nonuniform microstructure of sample L1. A bright surface is shown in Fig. 3d, indicating the absence of burn. Smearing is obvious in Fig. 3e, and several grinding grooves are present, except the subtle grinding marks. When the feed rate reached 10 μm/min, grinding burn happened, as illustrated in Fig. 3f. The surface roughness R_a was 1.1 nm at a feed rate of 5 μm/min, then decreasing to 0.7 nm with an increasing feed rate to 8 μm/min, indicating the instability of grinding performance produced by sample L1.

Figure 4 shows the optical and SEM images of sample M2, its EDS spectrum, optical and SEM images on a ground Si wafer, and surface roughness R_a and PV values as a function of feed rate on the Si wafers ground by sample M2. The weight percentage of magnesium oxide (MgO) is 13% (Table 1), which agrees well with the EDS spectrum in Fig. 4c, leading to the difficulty to identify the MgO powders in Fig. 4b. A bright surface is shown on the ground Si surface by sample M2 at a feed rate of 15 μm/min (Fig. 4d). The ground surface is clear in Fig. 4e, absent from smears observed in Fig. 3e, and subtle grinding marks are found, indicating the effectiveness of diamond grains in sample M2. Bright surfaces are obtained with increasing feed rates from 5 to 15 μm/min. Surface roughness R_a fluctuates from 1.3 to 1.7 nm, with increasing feed rates from 5 to 15 μm/min, corresponding to the PV values increasing from 11 to 15 nm.

Table 2 lists the surface roughness R_a changes from 0.85 to 0.97 nm, with increasing feed rates from 5 to 15 μm/min induced by sample C3, corresponding to the PV fluctuating from 8.3 to 11.38 nm. In this range, the ground surfaces of the Si wafers are bright, meaning the absence of burn. Sample C3 has the best grinding performance among three kinds of developed diamond wheels. Hereby, the grinding characteristics of sample C3 are investigated in a more detailed manner.

Figure 5 shows the surface roughness and morphology on the Si wafers ground by sample C3. Subtle grinding marks are illustrated on both the Si wafers, indicating the grinding effectiveness of diamond grains in sample C3. Surface roughness

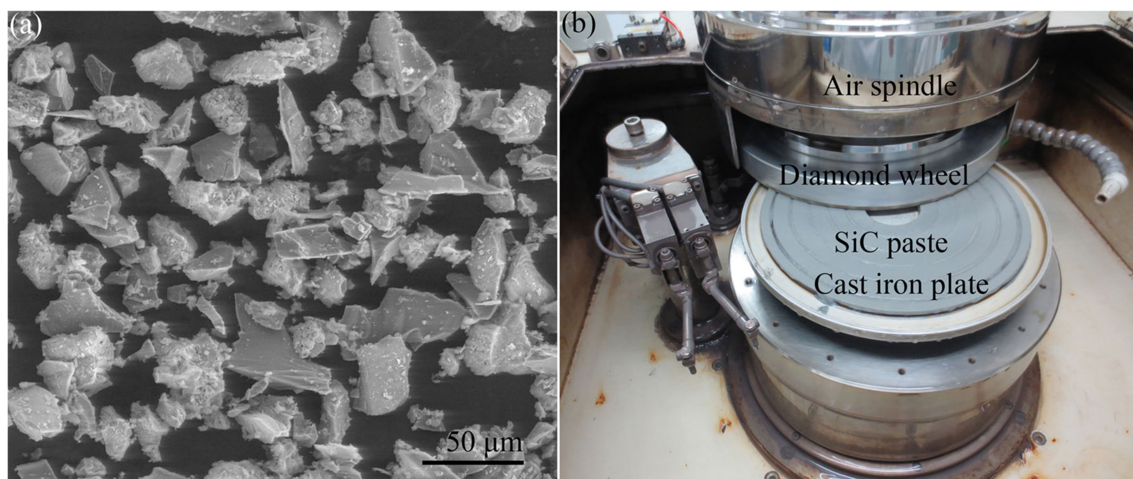

Fig. 2 SEM of SiC powders (**a**) and its paste (**b**) for truing a developed diamond wheel

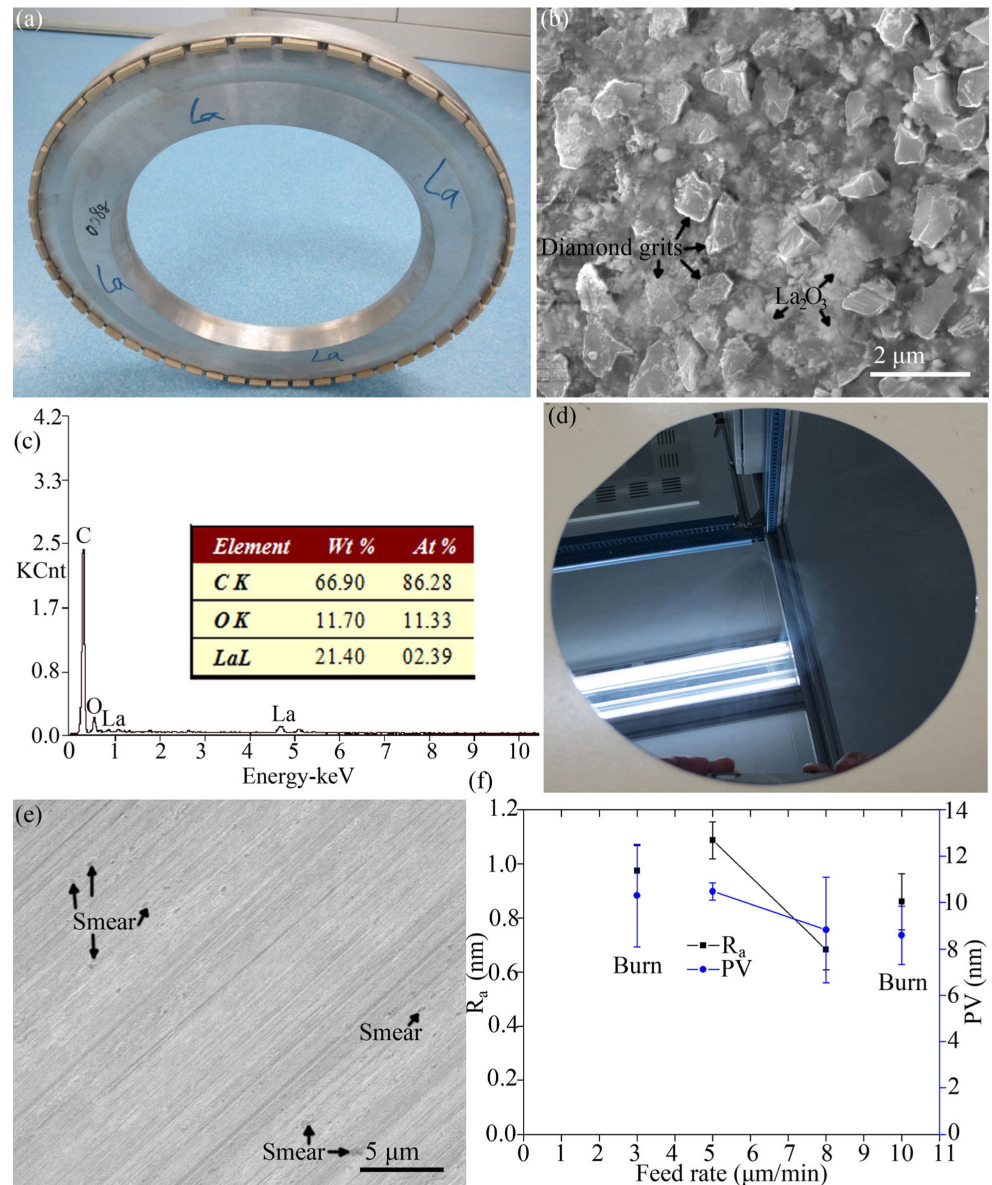

Fig. 3 **a** Optical and **b** SEM images of sample L1, **c** its EDS spectrum in **b**, **d** optical and **e** SEM images on a ground Si wafer at a feed rate of 8 µm/min, and **f** surface roughness R_a and PV as a function of feed rate on the Si wafers ground by sample L1

R_a and PV are 0.81 and 10.6 nm, respectively, at a feed rate of 8 µm/min, corresponding to those of 0.73 and 7.5 nm at a feed rate of 15 µm/min.

Figure 6 shows the surface roughness R_a and PV as a function of feed rate of sample C3. Surface roughness R_a and PV fluctuated in narrow ranges of 0.12 and 3.08 nm on the bright Si wafers, respectively, with increasing feed rates from 5 to 15 µm/min, except the burnt surfaces. These are the smallest fluctuation ranges and the most stable grinding performance among the three samples L1, M2, and C3. Surface roughness R_a and PV are 0.85 and 9.0 nm, respectively, at a feed rate of 8 µm/min, corresponding to those of 0.88 and 8.3 nm at a feed rate of 15 µm/min. Surface roughness R_a is less than 1 nm produced by sample C3, with increasing feed rates from 5 to 15 µm/min.

Figure 7 shows the SEM images of surface morphology and the corresponding EDS spectrum of sample C3. Phenolic resin was the bond material, and the microstructure was compact, as displayed in Fig. 7a, b. The weight percentage of ceria (CeO_2) was 25.5%, which is also identified in the EDS spectrum in Fig. 7c. CeO_2 powders are found in Fig. 7b with sizes varying from 100 to 200 nm, dispersing individually, which is different from the agglomerating of La_2O_3 powders in sample L1 (Fig. 3b). This is significant in achieving stabilized grinding performance.

Figure 8 shows the optical image and its EDS spectrum of a Si wafer ground by sample C3. The ground Si wafer was bright, showing a mirror surface finish, as illustrated in Fig. 8a. Si element is determined by the EDS spectrum on the Si wafer (Fig. 8b), free of oxygen element.

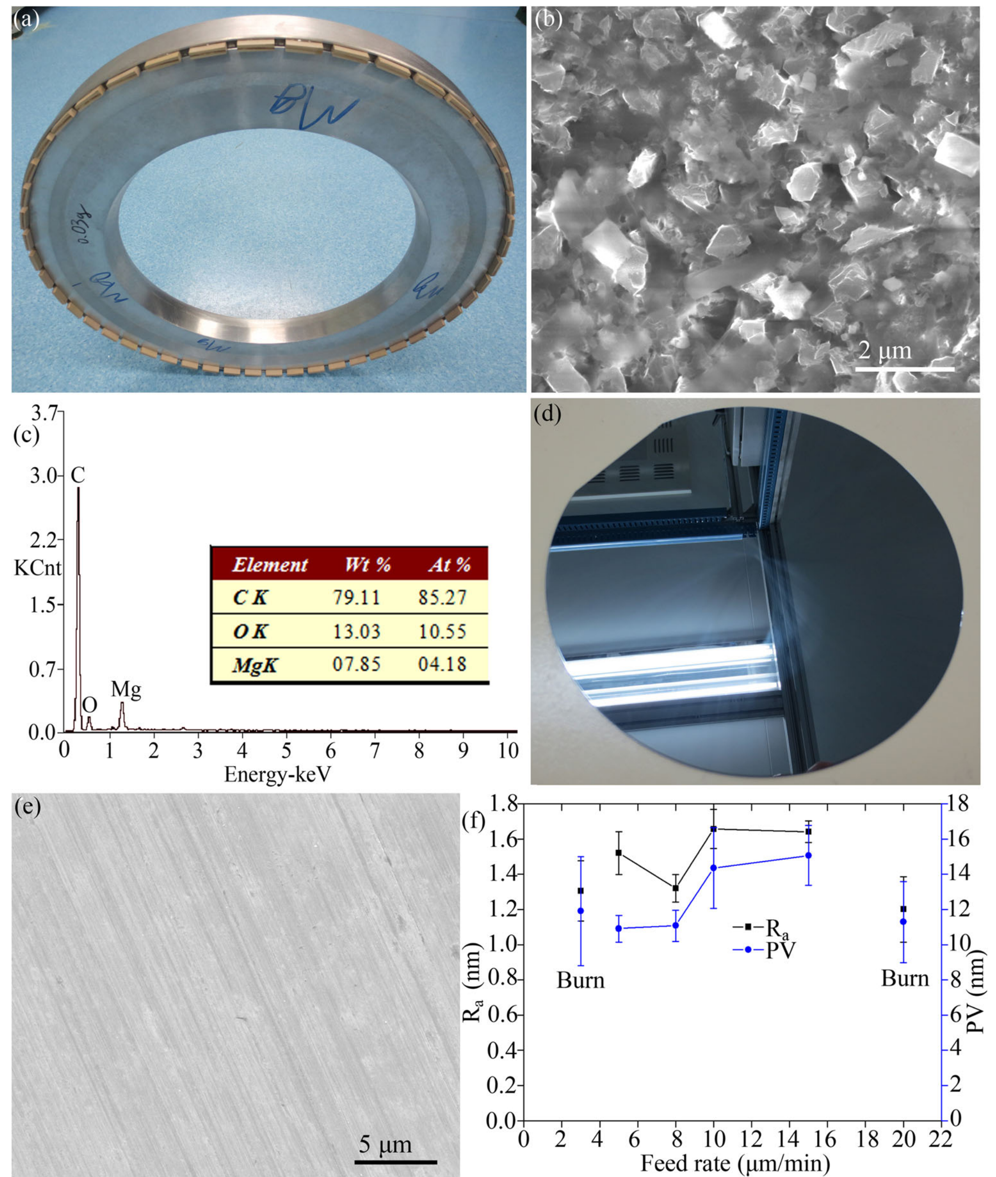

Fig. 4 **a** Optical and **b** SEM images of sample M2, **c** its EDS spectrum in **b**, **d** optical and **e** SEM images on a ground Si wafer at a feed rate of 8 μm/min, and **f** surface roughness R_a and PV as a function of feed rate on the Si wafers ground sample M2

Figure 9 shows the SEM images of Si wafers at different feed rates formed by sample C3. All the SEM images reveal subtle grinding marks and crack-free surfaces, indicating the ductile grinding on the Si surfaces induced by sample C3. Smears were absent from the Si wafers ground by sample C3 as depicted

Table 2 Surface roughness and calculated undeformed chip thickness of sample C3

Sample	Feed rate of wheel (μm/min)	Surface roughness (nm)		Calculated undeformed chip thickness (nm)
		R_a	PV	
C3	3	0.41 ± 0.03	4.89 ± 0.39	0.47
	5	0.88 ± 0.15	11.38 ± 2.33	0.61
	8	0.85 ± 0.07	9.02 ± 1.35	0.77
	10	0.97 ± 0.08	10.10 ± 1.34	0.86
	15	0.88 ± 0.11	8.30 ± 0.91	1.05
	20	0.64 ± 0.02	8.85 ± 1.25	1.21

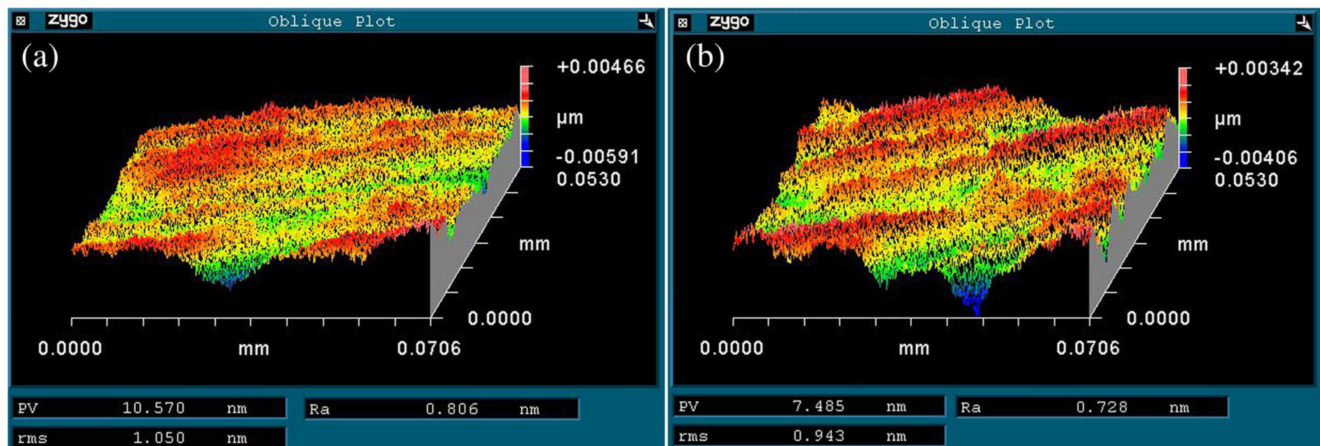

Fig. 5 Surface roughness and morphology on Si wafers ground by sample C3 at feed rates of **a** 8 and **b** 15 μm/min, respectively

in the SEM images, which were different from those generated by sample L1.

Figure 10 shows the cross-sectional TEM images of a Si wafer at a feed rate of 8 μm/min ground by sample C3. A uniform amorphous phase is at the top with thickness of 43 nm, as observed in Fig. 10a, followed by pristine crystalline lattice beneath (Fig. 10b–d). This is different from previous reports consisting of nanoindentation [11, 12], nanoscratch [13–15], and ultraprecision grinding [6, 16, 17], in which there are an amorphous top layer and a crystalline damaged layer underneath. Accordingly, a solely amorphous layer is achieved on the Si wafers using a developed diamond wheel. This is consistent with the results from the high-speed scratching studies using the diamond tips [7, 8]. In addition, selected area electron diffraction (SAED) pattern exhibits perfect Si-I phase, as illustrated in the inset of Fig. 10a, indicating an absence of high-pressure phases. This is in a good agreement with the findings from the high-speed scratching studies using the diamond tips [2, 3], but different from the previous reports of nanoindentation [11, 12] and nanoscratch [14, 15].

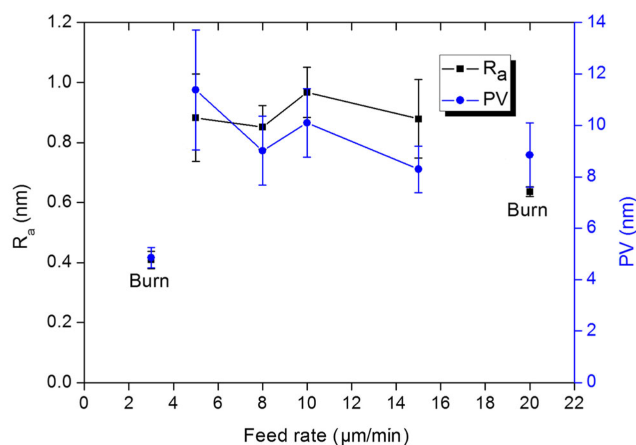

Fig. 6 Surface roughness R_a and PV as a function of feed rate of sample C3

Figure 11 shows the cross-sectional TEM images of a Si wafer at a feed rate of 15 μm/min induced by sample C3. The solely amorphous layer was 47 nm in thickness at the top (Fig. 9a), and the pristine crystalline lattice was at the bottom (Fig. 9b–f). There was no crystalline damaged layer beneath the amorphous phase, which is different from what has been reported in the previous literatures, in which an amorphous phase was at the top, followed by a crystalline damaged layer underneath [6, 11–17]. Additionally, SAED pattern shows the perfect Si-I phase in the inset of Fig. 11a, which is different from the high-pressure phases found in nanoindentation [11, 12] and nanoscratch [14, 15], such as Si-III and Si-XII phases. Thus, a novel approach of high-performance grinding is proposed to grind Si wafers with the presence of the solely amorphous layer using diamond wheels, which agrees well with the prediction of single-point diamond scratching at a high speed.

4 Discussion

The volume ratios of the diamond grains, additive, and phenolic resin were 37.5, 12.5–13.5, and 49–50%, respectively, in each developed diamond wheel, as listed in Table 1. For the grinding performance, the sequence is samples L1, M2, and C3 from the worst to the best, as shown in Figs. 1, 2, and 4, respectively. Sample C3 achieved the best grinding performance with CeO_2, whereas sample L1 obtained the worst with La_2O_3. To analyze the fundamental mechanisms, schematic diagrams of grinding for sample C3 are illustrated in Fig. 12. For a comparison, grinding with a ceramic

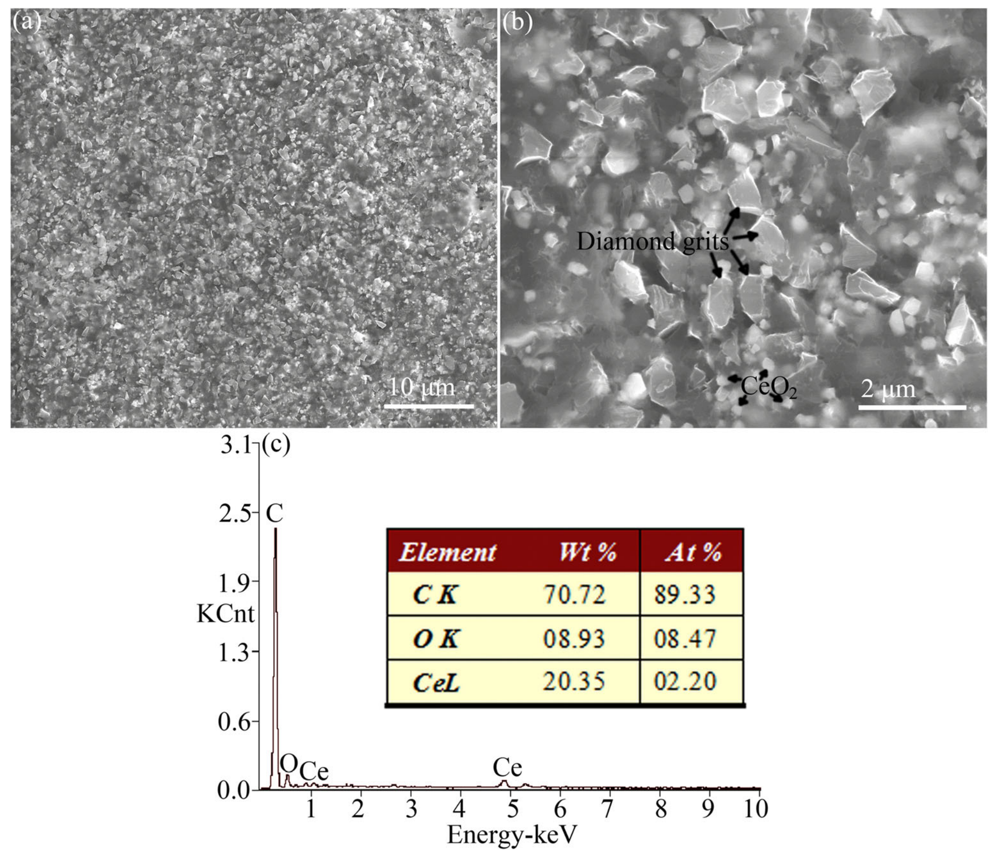

Element	Wt %	At %
C K	70.72	89.33
O K	08.93	08.47
CeL	20.35	02.20

Fig. 7 SEM images of surface morphology at low (**a**) and high (**b**) magnifications and its corresponding EDS spectrum in **b** of sample C3

bond diamond wheel is presented in Fig. 12d. Phenolic resin is soft and acts like springs during grinding (Fig. 12c). The diamond grains act moderately when exerted a vertical grinding force at the feed of grinding wheels. This relieves the aggression of the diamond grains on the Si surfaces, benefiting for achieving the solely amorphous layer. Even that, the diamond grains perform the grinding, which is confirmed by the grinding marks induced by samples L1, M2, and C3 in Figs. 3, 4, and 11, respectively. On the other hand, the ceramic bond is hard and provides a rigid support (Fig. 12d). During grinding, the diamond grains penetrate downwards, forming an amorphous layer top and a crystalline damaged layer beneath in a ground Si wafer, as found in the case of ultraprecision grinding [6, 16, 17].

CeO_2 has unique mechanical and chemical characteristics, compared with those of La_2O_3 and MgO [18–20]. It is widely used in the SiO_2 polishing and achieves the highest polishing rate [21, 22] among La_2O_3, Al_2O_3,

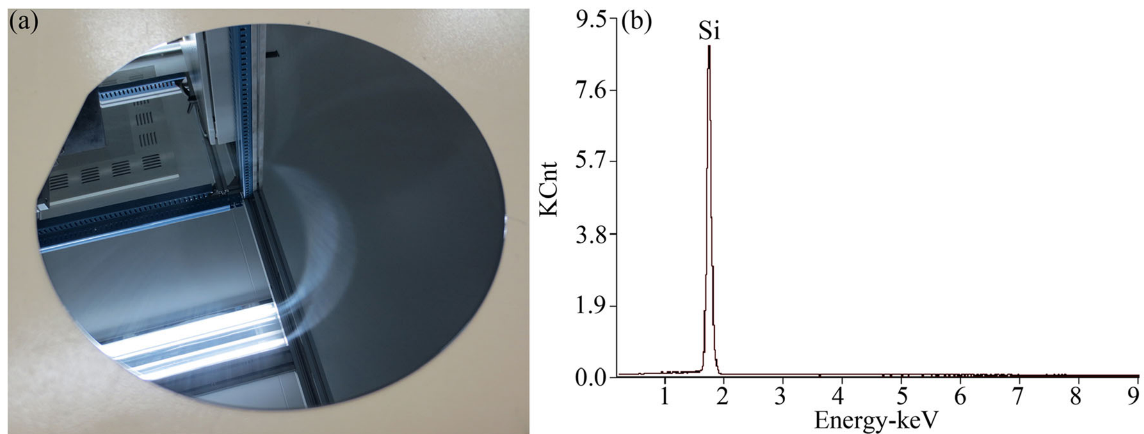

Fig. 8 Optical image (**a**) and its EDS spectrum (**b**) of a Si wafer ground by sample C3 at a feed rate of 15 μm/min

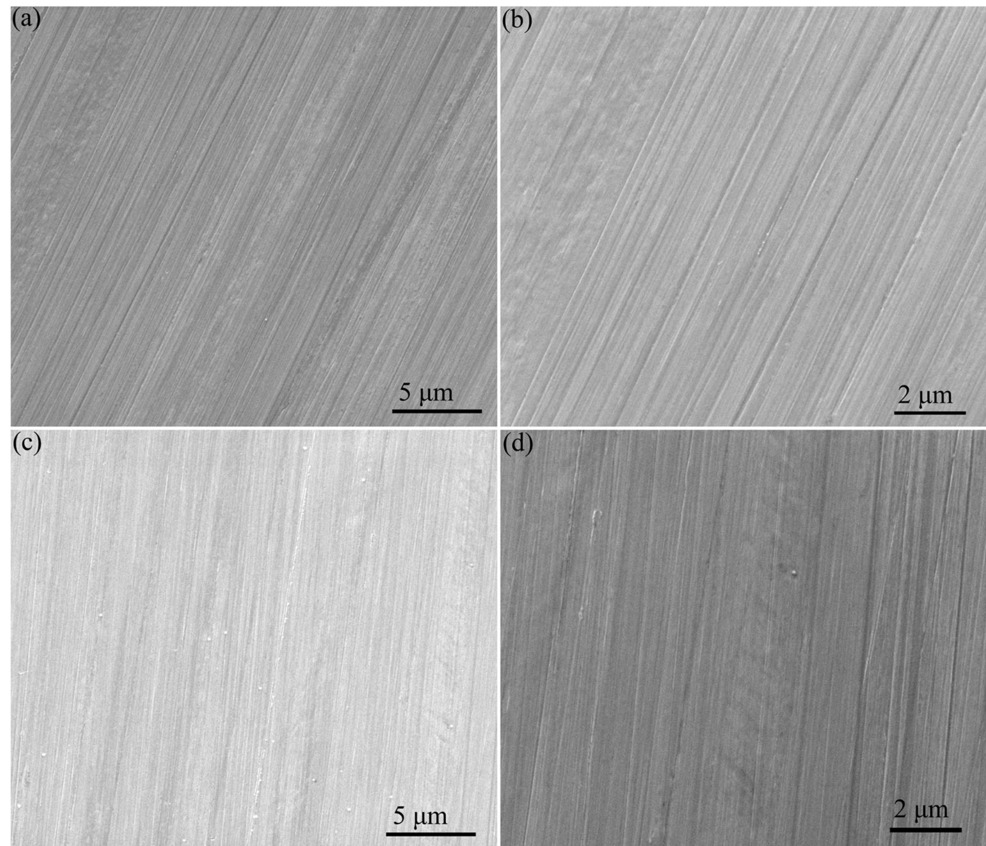

Fig. 9 SEM images on Si wafers ground by sample C3 at feed rates of **a**, **b** 8 and **c**, **d** 15 μm/min at low (**a**, **c**) and high (**b**, **d**) magnifications

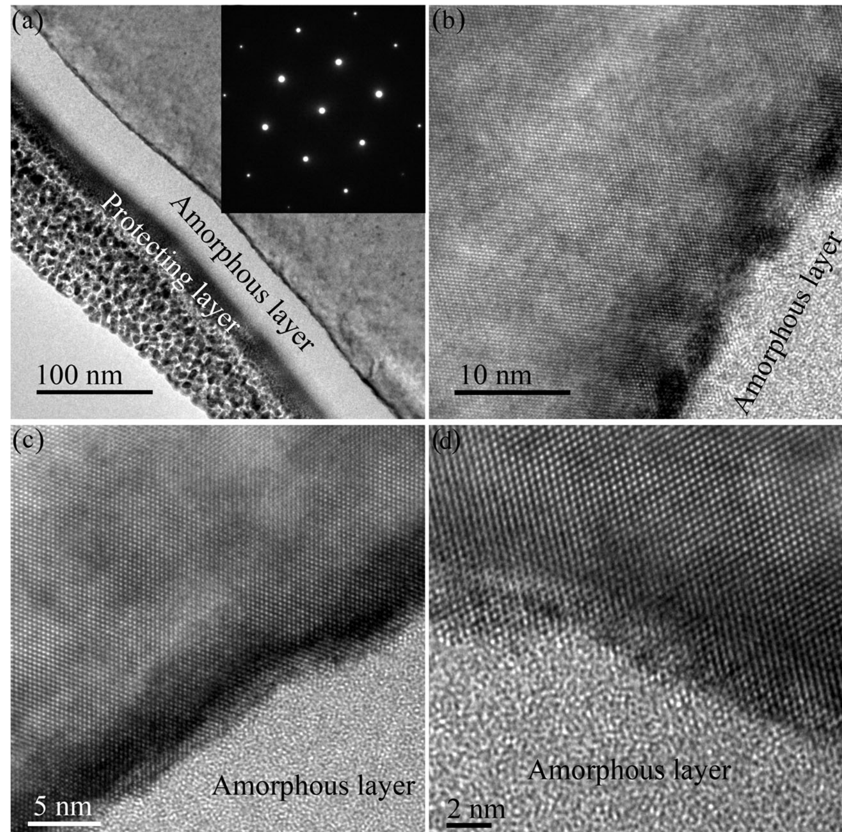

Fig. 10 Cross-sectional TEM images of a Si wafer ground by sample C3 at a feed rate of 8 μm/min at low (**a**) and high (**b**–**d**) magnifications. *Inset* in **a** showing its corresponding SAED pattern

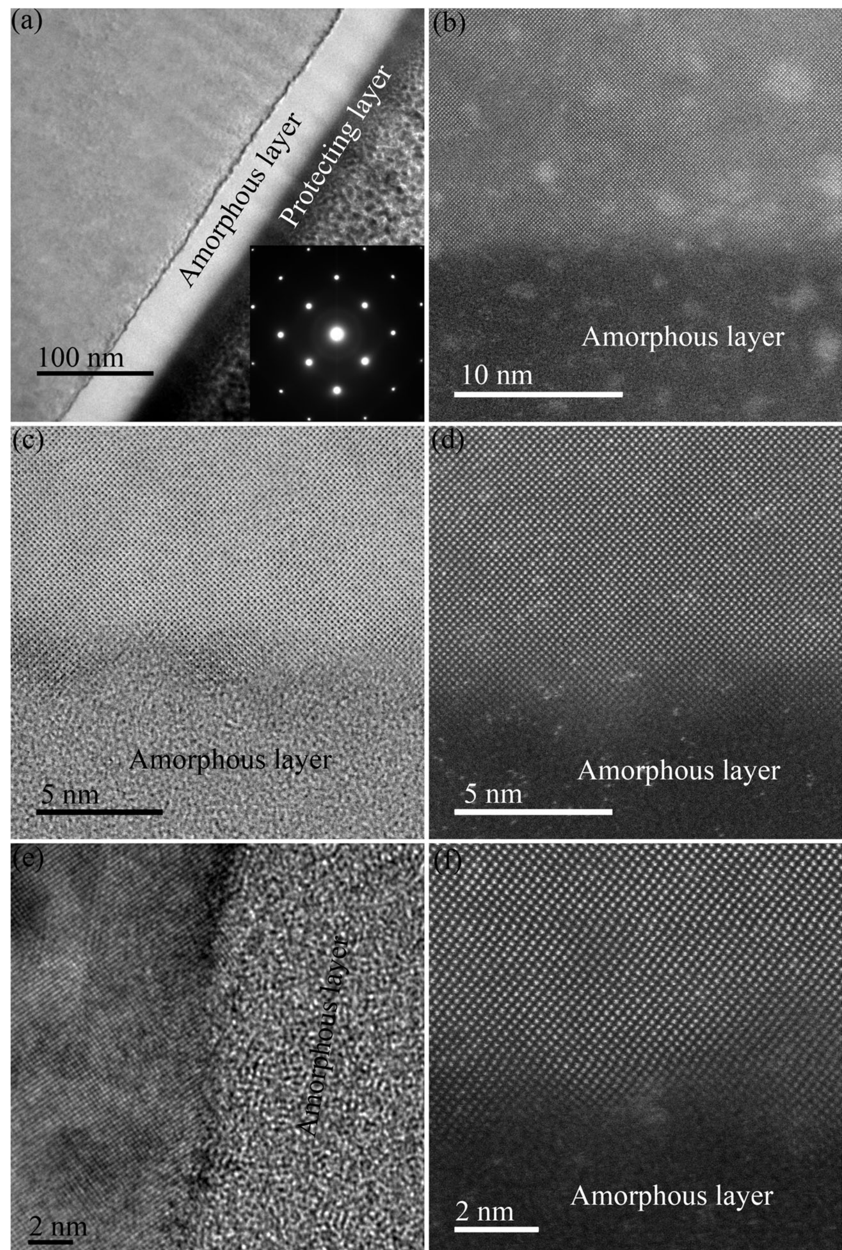

Fig. 11 Cross-sectional TEM images of a Si wafer ground by sample C3 at a feed rate of 15 μm/min in bright (**a**, **c**, **e**) and dark (**b**, **d**, **f**) fields at low (**a**) and high (**b**–**f**) magnifications. *Inset* in **a** showing its corresponding SAED pattern

Y_2O_3, TiO_2, ZrO_2, Cr_2O_3, and SnO_2 abrasives [21]. CeO_2 (melting point of 2400 °C) is softer than SiO_2, inflicting less damage on the Si surfaces than other abrasives mentioned previously [21, 22]. Si wafers are exposed in air, and the following equation takes place:

$$Si + O_2 \rightarrow SiO_2 \quad (1)$$

Therefore, there is an ultrathin layer of SiO_2 on the Si surfaces. CeO_2 is soft and achieves high polishing rate, which is attributed to the reduction reaction from Ce^{4+} to trivalent Ce^{3+} activated under mechanical force and thermodynamics effects induced by grinding [20, 21]. At the elevated temperature generated by grinding, CeO_2 reacts with deionized water used for coolant [19],

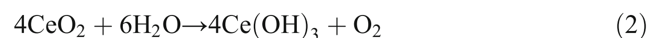

$$4CeO_2 + 6H_2O \rightarrow 4Ce(OH)_3 + O_2 \quad (2)$$

Under mechanical force produced by grinding, Si–O–Ce bonding forms at the interface between CeO_2 and SiO_2 [18, 19]. Si reacts with oxygen and CeO_2 at elevated temperature and mechanical force [18],

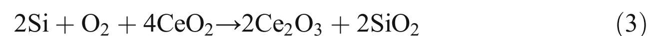

$$2Si + O_2 + 4CeO_2 \rightarrow 2Ce_2O_3 + 2SiO_2 \quad (3)$$

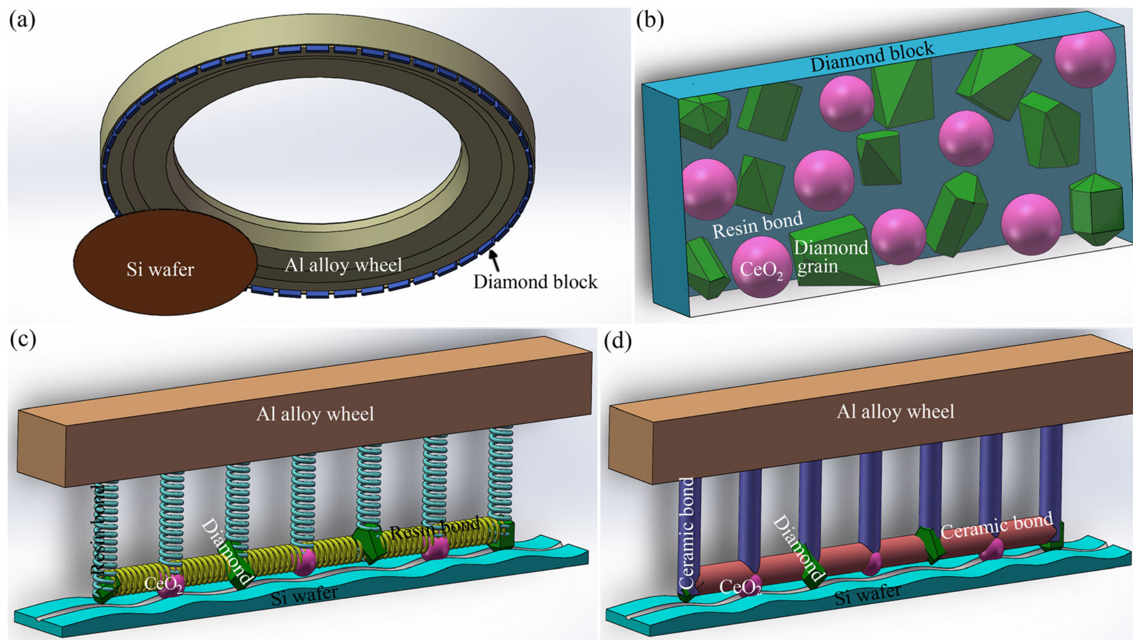

Fig. 12 Schematic diagrams of **a** face grinding on a Si wafer, **b** a diamond block of sample C3, **c** grinding using sample C3, and **d** grinding by a ceramic bond diamond wheel with CeO_2

During grinding, the mechanical force results in the breaking of O bonds in SiO_2 [20] and accelerates the chemical reaction at the CeO_2-SiO_2 interface. This leads to transferring of the electrons from the p-orbital of O atoms to the f-orbital of Ce atoms, resulting in the bonding of Si–O–Ce among dangling bonds of O atoms [20]. This accompanies the reduction reaction of Ce elements from Ce^{4+} to Ce^{3+} valent states. After the bonding, the SiO_2 lump is pulled out from the SiO_2 layer, leading to a high feed rate of a diamond wheel without burn on the Si surfaces. On the other hand, deionized water is present, and ionic reaction happens [19],

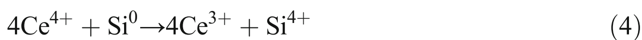

$$4Ce^{4+} + Si^{0} \rightarrow 4Ce^{3+} + Si^{4+} \quad (4)$$

Si^{4+} ions are easy to eliminate in the form of silicates.

Compared to CeO_2, the other two additives of La_2O_3 and MgO have no variation in chemical valent states during grinding, leading to the relatively worse grinding performance. La_2O_3 has hexagonal layer structure, providing lubrication function [23, 24]. This alleviates the rubbing of resin bond during grinding. La_2O_3 powders agglomerate in sample L1 (Fig. 3b), and they are crushed into debris with lubrication effect on the Si wafers under grinding force [23], resulting in the smears found in Fig. 3e. This contaminates the Si surfaces, increasing the cost and time of subsequent cleaning, because the lubrication effect of La_2O_3 dominates during grinding, leading to the unstable grinding performance (Fig. 3f) and smears left on the Si wafers (Fig. 3e). The hardness of MgO is 5.5 in Mohs hardness, which is less than 7 of SiO_2 [25]. Consequently, MgO is softer than SiO_2. For this reason, chemical reaction is dominant between the MgO and SiO_2, and otherwise, sample L1 would burn the Si wafers or give rise to a low feed rate. Accordingly, the reaction between MgO and SiO_2 is expressed at an elevated temperature induced by grinding,

$$MgO + SiO_2 \rightarrow MgSiO_3 \quad (5)$$

Thus, SiO_2 turns into silicate, and it is soluble and easy to eliminate in deionized water. The chemical reaction of MgO is not effective as the reduction reaction of CeO_2 forms Ce^{4+} to $Ce3^{+}$, forming the higher surface roughness of the former than the latter (Figs. 4f and 6).

The maximum undeformed chip thickness, h_m, is related to the grinding energy and used to characterize the effect of grinding conditions, as well as grinding performance [6, 16, 17]. The volume percentage of diamond grains in a diamond wheel, v, is 37.5% and calculated [16, 17]

$$v = \frac{4\pi}{3}\left(\frac{d_g}{2}\right)^3\left(\frac{C}{f}\right)^{1.5} \quad (6)$$

where C is the amount of surface active grains per unit area and f is 0.5 [13, 14], defining a ratio of active grains to the total grains on the surface. Then, Eq. (6) recasts

$$C = \frac{4f}{d_g^2\left(\frac{4\pi}{3v}\right)^{2/3}} \quad (7)$$

d_g is 760 nm calculated according to Eq. (8) [26]

$$d_{\mathrm{g}}(\mathrm{mm}) = \frac{15.2}{M} \tag{8}$$

where d_g is the equivalent grain diameter and M is the mesh size of a diamond wheel.

The h_{m} is expressed [16, 17],

$$h_{\mathrm{m}} = \frac{E_1}{E_2}\left(\frac{4}{rC^{1.5}}\frac{v_{\mathrm{f}}}{v_{\mathrm{s}}}\right)^{0.5} \tag{9}$$

where E_1 and E_2 are the elastic moduli of the diamond wheel and workpiece, respectively, r is the ratio of the width to thickness of an undeformed chip, v_{f} is the feed rate of a diamond wheel, and v_{s} is the wheel speed. r is 1.49 [17]. The hardness and elastic modulus of sample C3 are 1.26 ± 0.1 and 31 ± 1 GPa, respectively, measured by a TI 950 nanomechanical instrument. The elastic modulus of Si (100) is 150.2 ± 15.3 GPa [27]. The calculated maximum undeformed chip thickness of sample C3, h_{m}, increases monotonically from 0.47 to 1.21 nm with increasing feed rates from 3 to 20 μm/min, as listed in Table 2. The h_{m} is 0.77 nm at a feed rate of 8 μm/min, which is smaller than 1.05 nm at 15 μm/min, resulting in the lower thickness of the solely amorphous layer of the former (43 nm) than the latter (47 nm), as confirmed in Figs. 10 and 11, respectively. The undeformed chip thickness is at the level of angstrom, except for a feed rate of 15 μm/min, contributing greatly for achieving the solely amorphous layer (Figs. 10 and 11). Moreover, when h_{m} decreases to a critical value, such as 0.47 nm, the grinding energy increases sharply, causing burn on the Si wafers produced by sample C3 (Fig. 6). When h_{m} reaches 1.21 nm, the synergistic effect between reduction reaction and mechanical removal could not satisfy the high feed rate of 20 μm/min induced by sample C3, rubbing dominating and causing burn on the Si wafers (Fig. 6).

5 Conclusions

In summary, the additives of La_2O_3, MgO, and CeO_2 are used to develop samples L1, M2, and C3, respectively. From the best to the worst, a sequence of grinding performance is samples C3, M2, and L1. The CeO_2 powders disperse individually in sample C3, contributing to the best grinding performance, which is different from the agglomeration of La_2O_3 powders in sample L1. Smears are present and the surface roughness is unstable on the ground Si wafers produced by sample L1. By using sample M2, bright surfaces are obtained and their surface roughness R_{a} varies from 1.3 to 1.7 nm, with increasing feed rates from 5 to 15 μm/min. Surface roughness R_{a} varies from 0.85 to 0.97 nm, and PV changes from 8.3 to 11.38 nm on the bright Si wafers, with increasing feed rates from 5 to 15 μm/min ground by sample C3. The solely amorphous layer is achieved in thickness of 43 nm, at a feed rate of 8 μm/min of sample C3.

Acknowledgements The authors acknowledge the financial supports from the Excellent Young Scientists Fund of NSFC (51422502), Integrated Program for Major Research Plan of NSFC (91323302), Science Fund for Creative Research Groups of NSFC (51621064), Changjiang Scholars Program of Ministry of Education of China, Program for New Century Excellent Talents in University (NCET-13-0086), the Fundamental Research Funds for the Central Universities (DUT14YQ215), the Tribology Science Fund of State Key Laboratory of Tribology (SKLTKF14A03), Tsinghua University, the Science Fund of the State Key Laboratory of Metastable Materials Science and Technology (201501), Yanshan University, the Xinghai Science Funds for Distinguished Young Scholars and Thousand Youth Talents at Dalian University of Technology, the Natural Science Foundation of Jiangsu Province (BK20151190), Distinguished Young Scholars for Science and Technology of Dalian City (2016RJ05), and the Collaborative Innovation Center of Major Machine Manufacturing in Liaoning.

References

1. Pei ZJ, Fisher GR, Liu J (2008) Grinding of silicon wafers: a review from historical perspectives. Int J Mach Tools Manuf 48:1297–1307
2. Dai JB, Ding WF, Zhang LC, Xu JH, Su HH (2015) Understanding the effects of grinding speed and undeformed chip thickness on the chip formation in high-speed grinding. Int J Adv Manuf Technol 81:995–1005
3. Segal M (2012) Material history learning from silicon. Nature 483: S43–S44
4. Zhang ZY, Wang B, Zhou P, Guo DM, Kang RK, Zhang B (2016) A novel approach of chemical mechanical polishing using environment-friendly slurry for mercury cadmium telluride semiconductors. Sci Rep 6:22466
5. Zhang ZY, Yang S, Guo DM, Yuan BY, Guo XG, Zhang B, Huo YX (2015) Deformation twinning evolution from a single crystal in a face-centered-cubic ternary alloy. Sci Rep 5:11290
6. Zhang ZY, Huo FW, Wu YQ, Huang H (2011) Grinding of silicon wafers using an ultrafine diamond wheel of a hybrid bond material. Int J Mach Tools Manuf 51:18–24
7. Zhang ZY, Wang B, Kang RK, Zhang B, Guo DM (2015) Changes in surface layer of silicon wafers from diamond scratching. CIRP Ann Manuf Technol 64:349–352
8. Zhang ZY, Guo DM, Wang B, Kang RK, Zhang B (2015) A novel approach of high speed scratching on silicon wafers at nanoscale depths of cut. Sci Rep 5:16395
9. Ding WF, Xu JH, Chen ZZ, Yang CY, Song CJ, Fu YC (2013) Fabrication and performance of porous metal-bonded CBN grinding wheels using alumina bubble particles as pore-forming agents. Int J Adv Manuf Technol 67:1309–1315
10. Ma CY, Ding WF, Xu JH, Fu YC (2015) Influence of alumina bubble particles on microstructure and mechanical strength in porous Cu-Sn-Ti metals. Mater Des 65:50–56
11. Zarudi I, Zou J, Zhang LC (2003) Microstructures of phases in indented silicon: a high resolution characterization. Appl Phys Lett 82:874–876

12. Wong S, Haberl B, Williams JS, Bradby JE (2015) Phase transformation as the single-mode mechanical deformation of silicon. Appl Phys Lett 106:252103
13. Takagi M, Onodera K, Matsumuro A, Iwata H, Sasaki K, Saka H (2008) TEM and HRTEM observations of microstructural change of silicon single crystal scratched under very small loading forces by AFM. Mater Trans 49:1298–1302
14. Gassilloud R, Ballif C, Gasser P, Buerki G, Michler J (2005) Deformation mechanisms of silicon during nanoscratching. Phys Status Solidi A Appl Mater 202:2858–2869
15. Wu YQ, Huang H, Zou J, Zhang LC, Dell JM (2010) Nanoscratch-induced phase transformation of monocrystalline Si. Scripta Mater 63:847–850
16. Zhang ZY, Huo FW, Zhang XZ, Guo DM (2012) Fabrication and size prediction of crystalline nanoparticles of silicon induced by nanogrinding with ultrafine diamond grits. Scripta Mater 67:657–660
17. Zhang ZY, Huo YX, Guo DM (2013) A model for nanogrinding based on direct evidence of ground chips of silicon wafers. Sci China Technol Sci 56:2099–2108
18. Zhou L, Eda H, Shimizu J, Kamiya S, Iwase H, Kimura S (2006) Defect-free fabrication for single crystal silicon substrate by chemo-mechanical grinding. CIRP Ann Manuf Technol 55:313–316
19. Pineiro A, Black A, Medina J, Dieguez E, Parra V (2013) The use of potassium peroxidisulphate and Oxone (R) as oxidizers for the chemical mechanical polishing of silicon wafers. Wear 303:446–450
20. Rajendran A, Takahashi Y, Koyama M, Kubo M, Miyamoto A (2005) Tight-binding quantum chemical molecular dynamics simulation of mechano-chemical reactions during chemical-mechanical polishing process of SiO_2 surface by CeO_2 particle. Appl Surf Sci 244:34–38
21. Hoshino T, Kurata Y, Terasaki Y, Susa K (2001) Mechanism of polishing of SiO_2 films by CeO_2 particles. J Non-Cryst Solids 283:129–136
22. Feng XD, Sayle DC, Wang ZL, Paras MS, Santora B, Sutorik AC, Sayle TXT, Yang Y, Ding Y, Wang XD, Her YS (2006) Converting ceria polyhedral nanoparticles into single-crystal nanospheres. Science 312:1504–1508
23. Zhang ZY, Lu XC, Han BL, Luo JB (2007) Rare earth effect on the microstructure and wear resistance of Ni-based coatings. Mater Sci Eng A 454:194–202
24. Zhang ZY, Lu XC, Han BL, Luo JB (2007) Rare earth effect on microstructure, mechanical and tribological properties of CoCrW coatings. Mater Sci Eng A 444:92–98
25. Gao S, Dong ZG, Kang RK, Guo DM (2013) Design and evaluation of soft abrasive grinding wheels for silicon wafers. Proc Inst Mech Eng Part B J Eng Manuf 227:578–586
26. Malkin S, Guo CS (2008) Grinding technology: theory and applications of machining with abrasives, vol 2 . Industrial Press, New York, pp 14–15Ch 2
27. Ebrahimi F, Kalwani L (1999) Fracture anisotropy in silicon single crystal. Mater Sci Eng A 268:116–126